NANO LETTERS

Letter

pubs.acs.org/NanoLett

Tuning and Persistent Switching of Graphene Plasmons on a Ferroelectric Substrate

Michael D. Goldflam,*[,†] Guang-Xin Ni,[†,‡,$] Kirk W. Post,[†] Zhe Fei,[†] Yuting Yeo,[$] Jun You Tan,[$] Aleksandr S. Rodin,[†,‡] Brian C. Chapler,[†] Barbaros Özyilmaz,[‡,$] Antonio H. Castro Neto,[‡] Michael M. Fogler,[†] and D. N. Basov[†]

[†]Physics Department, University of California—San Diego, La Jolla, California 92093, United States

[‡]Centre for Advanced 2D Materials and Graphene Research Centre, National University of Singapore, Singapore 117546

[$]Department of Physics, National University of Singapore, 2 Science Drive 3, Singapore 117542

Supporting Information

ABSTRACT: We characterized plasmon propagation in graphene on thin films of the high-κ dielectric $PbZr_{0.3}Ti_{0.7}O_3$ (PZT). Significant modulation (up to ±75%) of the plasmon wavelength was achieved with application of ultrasmall voltages (< ±1 V) across PZT. Analysis of the observed plasmonic fringes at the graphene edge indicates that carriers in graphene on PZT behave as noninteracting Dirac Fermions approximated by a semiclassical Drude response, which may be attributed to strong dielectric screening at the graphene/PZT interface. Additionally, significant plasmon scattering occurs at the grain boundaries of PZT from topographic and/or polarization induced graphene conductivity variation in the interior of graphene, reducing the overall plasmon propagation length. Lastly, through application of 2 V across PZT, we demonstrate the capability to persistently modify the plasmonic response of graphene through transient voltage application.

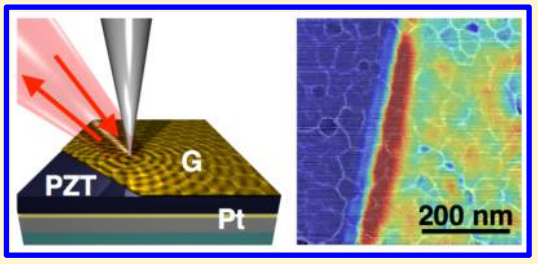

KEYWORDS: *graphene, ferroelectric, PZT, near-field microscopy, plasmonics, s-SNOM*

Graphene plasmonics is a burgeoning field of study that has attracted significant interest due to graphene's unique electronic and optical properties, as well as the ability to conveniently modify these properties through back-gating or optical pumping.[1−5] Extensive work has been performed to characterize the capabilities of different gate dielectrics for tuning of the electronic properties of graphene. Among the most studied gate dielectrics are SiO_2, for its robustness with voltage application, and hexagonal boron nitride (hBN), for the high mobility it lends to graphene microcrystals or films.[6−8] However, the realization of practical plasmonic devices requires implementation of alternative dielectrics to achieve larger variance in graphene properties and to potentially attain additional control mechanisms (e.g., persistent effects). Ferroelectrics are one intriguing option. In general, such dielectrics have a large DC permittivity (κ or ε_{DC}) in the linear, low-field regime and also may enable persistent tuning in the high-field nonlinear regime.[9−14] As a result, ferroelectrics may find applications in graphene-based electronics and plasmonics. Although previous experimental works on ferroelectric modification of graphene primarily investigated control of electronic properties,[9−19] we focus here on the plasmonic and photonic response. We examined the potential for tuning of the plasmonic response of graphene through the use of one such dielectric, $PbZr_{0.3}Ti_{0.7}O_3$ (PZT). The dielectric constant of PZT can reach values of several hundred or thousand, many times that of SiO_2, making it an extremely effective insulator for back-gated structures.[10] Therefore, PZT's potency for use in future plasmonic devices warrants investigation.

To characterize graphene plasmon propagation on PZT substrates, we employed scattering-type scanning near field optical microscopy (s-SNOM).[20−22] In these measurements, infrared light is focused at the sharp apex of a metallic atomic force microscope (AFM) tip as seen in Figure 1a (Neaspec).[23−25] A fraction of the incident radiation polarizes the tip and is confined to length scales on the order of the tip diameter (~20 nm) where the tip interacts with the sample. As a result, the light scattered from the tip-sample system contains information on the sample properties at deeply subdiffraction limited length scales.[24] Additionally, through the enhanced range of momenta excited by the tip,[5,26,27] it is possible to overcome the momentum mismatch between plasmonic modes and the incident far field light allowing the tip to launch radially propagating plasmons, which are reflected from topographic and electronic features in the graphene (e.g., edges, wrinkles, folds, grain boundaries) as shown schematically in Figure 1a.[23] These reflected waves create oscillations in the local electric field directly beneath the tip corresponding to a detected variation in near-field signal. Analysis of the oscillating near field signal yields information including the plasmon wave-

Received: January 11, 2015
Revised: July 9, 2015
Published: July 16, 2015

ACS Publications © 2015 American Chemical Society

DOI: 10.1021/acs.nanolett.5b00125
Nano Lett. 2015, 15, 4859−4864

Downloaded via UNIV OF CALIFORNIA SAN DIEGO on July 18, 2018 at 01:24:33 (UTC).
See https://pubs.acs.org/sharingguidelines for options on how to legitimately share published articles.

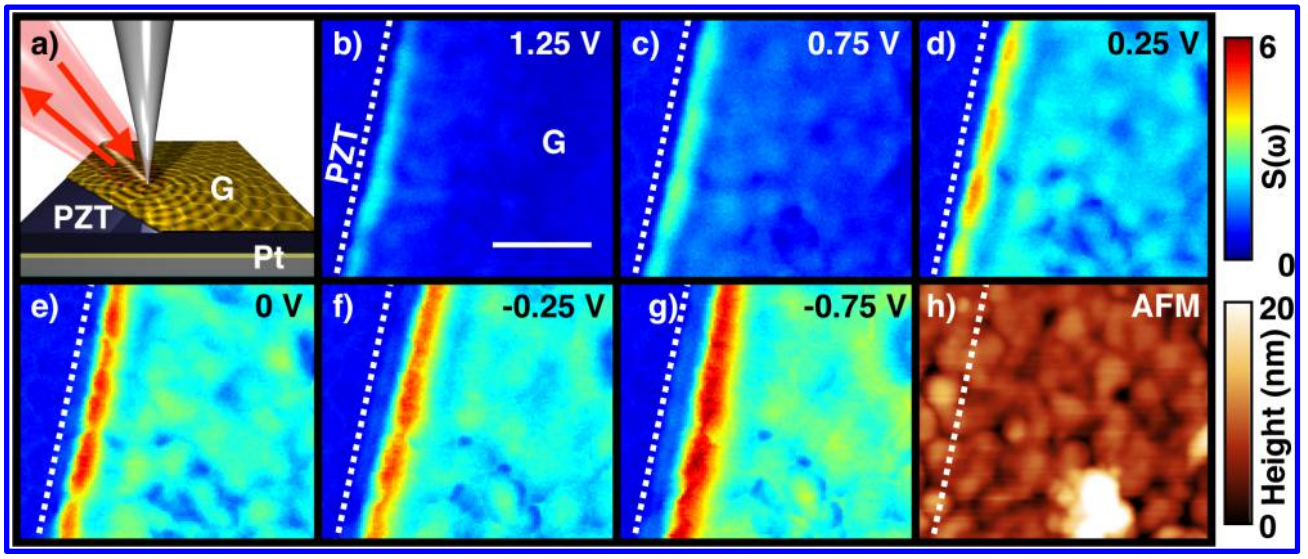

Figure 1. (a) Schematic of our nanoimaging setup. The concentric yellow circles represent propagating plasmonic waves launched by the tip and reflected by the graphene edge. (b–g) Normalized voltage dependent near-field amplitude ($S(\omega)$) of graphene (right) on PZT (left) taken at ω = 890 cm^{-1}. The dotted white line indicates the position of the graphene (denoted as G) edge determined from AFM. A strong plasmonic fringe is visible near this edge. Fringe brightness and width increase with decreasing voltage. (h) AFM image, taken simultaneously with the 0 V data, showing device roughness in the same region as the SNOM images shown in (b–g).

length (λ_p) given by twice its periodicity as seen in Figure 2, and corresponding damping coefficient, γ_p. Both these parameters are directly related to the properties of graphene, including the scattering rate and carrier density.[5,27]

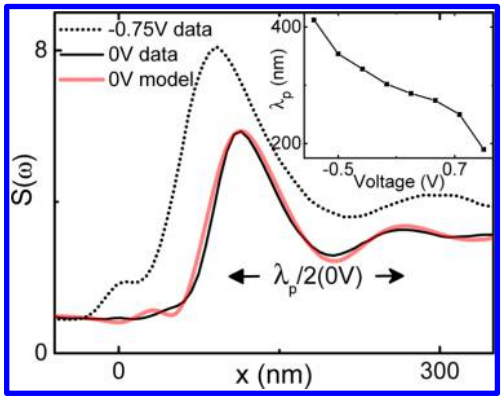

Figure 2. Comparison of simulated plasmonic profile (red) and data (solid black) taken from Figure 1d with 0 V applied to the back gate. There is good agreement between the two profiles for γ_p = 0.13. The profile for the longest wavelength data (dotted black) is also shown. (Inset) Gate-dependent plasmonic wavelength obtained from the images in Figure 1.

Our device consists of a graphene microcrystals exfoliated on a 360 nm-thick polycrystalline PZT film grown via sol gel on a 50 nm platinum layer that functions as our back-gate, as shown in the schematic in Figure 1a. This back-gated structure allows for straightforward carrier doping of graphene in the linear dielectric regime of PZT (-1 V < V_G < $+1$ V) during near-field measurements. To accurately probe graphene plasmons without the influence of plasmon–phonon coupling, which modifies the frequency–momentum dispersion of the graphene plasmon from the simple square-root dependence,[26] the sample was probed using a coherent infrared beam generated by a CO_2 laser at ω = 890 cm^{-1}, where no PZT phonons are present. We first characterized our device at back-gate voltages ranging from V_G = −0.75 V–1.25 V, where negative and positive voltages indicate an increase or decrease in the hole concentration in the graphene. The resulting normalized near field amplitudes are shown in Figure 1b–g. In these images, the near field signal is related to the local z component of the electric field (E_z) beneath the tip, with higher signal generally relating to a higher E_z in graphene. An AFM image of the same region is shown in Figure 1h.

We first survey the gross features present in the near field images. The most prominent aspect of these images is the bright fringe seen at the edge (white dotted line across each image) of the graphene flake. According to previous studies,[5,27] they are formed due to interference between tip-launched and edge reflected plasmons. As the hole concentration (n), and therefore the graphene conductivity (σ), increases at more negative V_G, the width and intensity of these fringes, along with the overall graphene signal, monotonically grow in congruence with previous measurements of structures utilizing SiO_2 gate insulator. This monotonic change in n with V_G reveals that the Fermi energy (E_F) never crosses the charge neutrality point (CNP), which would correspond to a reduction and subsequent enhancement of n. Rather, this result suggests a positive carrier sign at all gate voltages in this range and indicates unintentional hole doping of the graphene at 0 V. From near-field measurements over a broader voltage range, we expect that the voltage at the CNP is between 1.0 and 1.5 V (see Supporting Information). This is consistent with a minimal carrier concentration at V_G = 1.25 V, resulting in the near invisibility of graphene in Figure 1b where only a weak fringe is visible, as charge neutral graphene is nearly infrared transparent, transmitting approximately 98% of incident light. The existence of a weak fringe in spite of low carrier concentration is likely due to edge doping, as was previously seen in graphene on SiO_2[28,29] and is also reflected in the decreasing overall signal in regions of graphene away from the edge.

To directly characterize plasmon behavior, we examined the near field signal close to the graphene edge where interference fringes are most prominent. The plasmon wavelength, λ_p, can

DOI: 10.1021/acs.nanolett.5b00125
Nano Lett. 2015, 15, 4859–4864

be directly extracted from the images in Figure 1b−g by obtaining a line profile of our SNOM signal perpendicular to the edge. Many such profiles are obtained and averaged to eliminate artifacts from variation in substrate topography and substrate optical properties. The resulting profile obtained from our 0 V data is plotted as the solid black curve in Figure 2. This profile shows characteristic fringes, which decrease in amplitude with increasing distance from the graphene edge. Modification of the applied voltage results in variation of the amplitude and wavelength of the interference fringes. The values of λ_p extracted from the averaged line profiles extracted at each applied voltage are shown in the inset of Figure 2. The measured wavelength varies by as much as ±75% of its value at 0 V with a voltage range of only ±1 V. This is more than 2 orders of magnitude greater than what is seen in SiO_2-supported graphene structures for the same range of applied electric fields.

The measurements reported in Figures 1 and 2 can serve as an alternative method for directly determining the DC dielectric constant of PZT. The theoretical plasmon dispersion can be calculated from the maximum of the reflection coefficient, $R_p(\omega = 890\ \mathrm{cm}^{-1})$, which has a well-defined dependence on the graphene carrier concentration.[1,5,26,30,31] A comparison of this theoretical dispersion and the measured plasmon wavelength allows for extraction of the graphene carrier concentration, n, at each applied voltage, V_G. This carrier density then yields the dielectric constant of PZT: $\varepsilon_{DC} = (ned/|V_G - V_{CNP}|)$ where e is the electron charge, d is the PZT thickness, and V_{CNP} = 1.3 V consistent with our near field measurements. This analysis yields a range of values ε_{DC} = 450−550, well within the expected range for PZT and in agreement with direct measurements on similar films.

In spite of the large wavelengths we observe in Figures 1 and 2, the plasmon propagation length appears limited to ∼500 nm even for the longest λ_p = 420 nm (black dotted line in Figure 2), indicating the presence of plasmonic scattering in these devices. Information on losses and scattering can be obtained by examining the decay in the interference fringe strength with increasing tip-to-edge distance. Although averaging many curves with slight variation in phase has the potential to mask intrinsic damping, a comparison of damping extracted from averaged and nonaveraged data shows little variation in the plasmonic damping. To obtain the plasmon damping coefficient, γ_p, we modeled our plasmonic profile obtained at V_G = 0 V using the procedure outlined in Fei et al.,[5] approximating the tip as an elongated ellipsoid.[32] The value of γ_p is varied until the theoretical fringe profile matches experimental data. The resulting simulated profile is shown by the red curve in Figure 2 and fits our experimental data (solid black) most closely for γ_p = 0.135. The measured damping and wavelength are directly related to the plasmon dispersion via $\lambda_p = 2\pi/q_1$ and $\gamma_p = q_2/q_1$ and complex graphene conductivity, $\sigma = \sigma_1 + i\sigma_2$, with the theoretical dispersion given by

$$q_p = q_1 + iq_2 = \frac{i\omega[1 + \epsilon(\omega)]}{4\pi\sigma(\omega)} \quad (1)$$

where ω = 890 cm^{-1} is the excitation frequency and $\epsilon(890\ \mathrm{cm}^{-1}) = 2.58 + 0.12i$ is the ellipsometrically measured permittivity of the PZT at our probing frequency. At V_G = 0 V, the measured plasmon wavelength (λ_p = 270 nm) and damping (γ_p =0.135) yield a graphene conductivity of $\sigma(890\ \mathrm{cm}^{-1}) = (0.56 + 5.8i) \times e^2/h$. The uncertainty in the extracted plasmon wavelength is ∼ ±30 nm and is a result of several factors including the tip radius (20 nm), which determines the resolution of our measurements. The conductivity, determined from near field data, can be compared to a semiclassical Drude model for graphene using a carrier relaxation rate, τ^{-1} = 70 cm^{-1}, determined independently from the DC mobility of μ = 2000 $\mathrm{cm}^2/(\mathrm{V{\cdot}s})$ measured using transport in single grains of chemical vapor deposition grown graphene.[10] The conductivity from this model is given by[33]

$$\sigma(\omega) = \frac{e^2 E_F}{\pi\hbar}\frac{i}{\omega + i\tau^{-1}} = (0.5 + 6.7i) \times e^2/h \quad (2)$$

where $E_F(0\ \mathrm{V})$ = 3000 cm^{-1} is the graphene Fermi energy. Plasmonic damping originates from a combination of losses within graphene itself and those resulting from the dielectric environment around graphene as given by $\gamma_p \approx \sigma_1/\sigma_2 + (\varepsilon_2/(1 + \varepsilon_1))$ with σ_1/σ_2 = 0.098 and $(\varepsilon_2/(1 + \varepsilon_1))$ = 0.037 giving the relative contributions from each channel. Additionally, the agreement between the noninteracting Drude model and our measured conductivity indicates that damping in the graphene can be ascribed to the high scattering rate of the electron gas in graphene on PZT. In this regime of enhanced scattering, the many body interactions that were previously reported for graphene on SiO_2[5] and BN[34] do not play a significant role. Additionally, the absence of many body effects in our device can be understood as a direct result of the high dielectric constant of PZT, which serves to screen electron−electron interaction reducing the overall strength of the Coulomb force by several orders of magnitude as compared to structures using SiO_2 as the gate insulator.[35]

Surprisingly, the value of the loss factor γ_p observed in our device is comparable to that measured by Fei et al.[5] However, in contrast to their results, it is difficult to distinguish fringes beyond the first directly in our imaging data. Examination of the internal regions of graphene shows the existence of bright fringes that are reminiscent of the plasmonic interference patterns observed at the edges of graphene flakes. These findings suggest the existence of plasmonic reflectors and scatterers within the interior of graphene, as these are a prerequisite for the formation of these additional interference patterns.[36] Initial examination of the data suggests a correlation between the underlying PZT grain topography and reflected plasmons. The AFM image in Figure 1h shows a similar topographic landscape on bare PZT and graphene covered PZT, indicating that graphene sits closely to the surface of PZT, directly following the grain structure below it. The surface roughness of PZT is ∼4 nm across the 1 × 1 μm region shown in Figure 1h with similar roughness reflected in the graphene. Individual PZT grains are visible in topography within both regions, with dimensions on the order of tens of nanometers.

To verify PZT grain boundaries as the source of plasmonic reflection within the interior of graphene, conventional Laplacian edge detection techniques were applied to the AFM data in Figure 1h resulting in the processed image in Figure 3a.[37,38] The white traces running throughout this panel indicate the edges of PZT grains. In order to determine the relationship between the bright fringes in the graphene interior and the PZT grains, we overlaid the near field image from Figure 1g on top of the processed AFM image to create Figure 3b. In this image, the PZT grain edges are simultaneously visible with the near field signal. The bright features in the

DOI: 10.1021/acs.nanolett.5b00125
Nano Lett. 2015, 15, 4859−4864

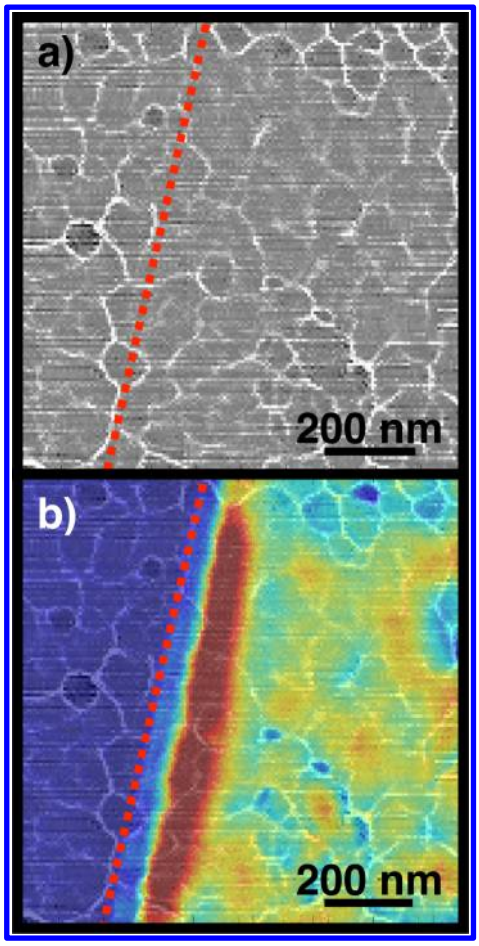

Figure 3. (a) Image obtained from conventional Laplacian edge detection techniques performed on topography from Figure 1h. Grain borders shown by white lines throughout image. (b) Near field signal from Figure 1g overlaid on the processed topography shown in (a).

interior of graphene appear to be enclosed within PZT grains suggesting that plasmons are reflected at the boundaries of these grains. This points to two possible sources of plasmonic reflection within the interior of graphene, both of which are governed by the existence of PZT grains: (1) topographic variation created in graphene by PZT creates strong enough variation in local graphene conductivity (from strain or other effects) to reflect plasmons and (2) different grains in PZT are polarized differently causing local conductivity changes which reflect plasmons. These two sources are difficult to distinguish with our current measurements, requiring alternative techniques, but do not modify the analysis described here.

For such analysis to hold, trivial topographical influence on near field signal[39] must be accounted for as topographic variation can modify the collected near field signal. In general, concave surface features create higher near field signal resulting from field enhancement, whereas convex surfaces result in lower signal. This is in contrast to what we observe with higher signal concentrated in the central convex regions of the PZT grains. Our analysis, therefore, suggests that PZT created graphene conductivity variation is a significant source of plasmonic reflection within the interior of graphene. Scattering from these local conductivity changes exacerbates the task of distinguishing multiple fringes close to the edge in the near field images without averaged profiles as the additional reflectors can deflect propagating plasmons before they are able to make the round trip from the tip to the edge and back. The observation of rapid plasmon decoherence in our near field images, compared with that in SiO_2 and resulting from scattering from PZT grains, suggests that significant improvement in the observed propagation length may be achieved by using graphene on atomically flat epitaxial PZT giving plasmons a smooth surface across which they can propagate.[12]

In spite of the significant scattering resulting from topographic features, we were able to employ ferroelectric switching of PZT for persistent tuning of graphene plasmons. As a ferroelectric material, PZT can be persistently polarized with application of transient electric fields greater than ~30 kV/cm (1 V across our device). It was previously demonstrated that this field application modifies the voltage of the graphene CNP, producing a corresponding change in the graphene carrier concentration and plasmonic characteristics, even after removal of the voltage.[9,10,13,40]

To test the possibility of plasmonic memory gating, we first obtained a near field image of an unpolarized region of the device at 0 V. After this measurement, a gate voltage of 2 V was applied for several minutes to polarize the PZT. Although the fairly low field from application of 2 V to our PZT film is not sufficient for complete polarization, it is larger than the coercive field of PZT and should therefore be enough to partially and persistently align the dipoles within the film (see Supporting Information). Following voltage removal, a second image was obtained in the same region of the device. Because the application of positive voltages reduces the hole concentration, any film polarization remaining after voltage application should result in a similar decrease in near field signal as that seen with increasingly positive V_G in our continuous bias application measurements in Figure 1b–g. The two near field images taken before and after memory gating, and their corresponding profiles, are shown in Figure 4a–d. Prior to voltage application,

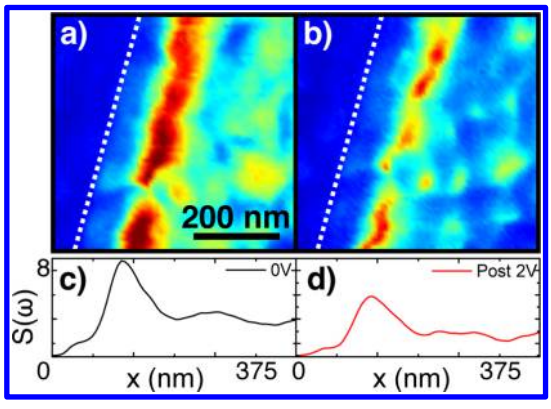

Figure 4. (a) Normalized near field amplitude of graphene on an unpolarized region of PZT. (b) Second image taken in the same region as (a) after application and removal of 2 V across PZT. (c) and (d) Line profiles corresponding to the plasmonic fringe seen in (a) and (b), respectively.

a bright fringe is visible in Figure 4a with multiple maxima seen in the corresponding line profile shown in Figure 4c. The equivalent data taken after voltage removal, Figure 4b and d, respectively, demonstrate significant reduction in fringe strength and overall graphene brightness, as well as the disappearance of the second fringe in the line profile. These changes are consistent with a reduction in the magnitude of graphene doping, a quantity to which our near-field data is

DOI: 10.1021/acs.nanolett.5b00125
Nano Lett. 2015, 15, 4859–4864

extremely sensitive. Thus, these data demonstrate the ability to persistently turn off the plasmonic response with transient voltage application. These changes to graphene carrier concentration were reversible with negative bias application and faded with extended 0 V bias application as seen in other ferroelectric based devices.[41] This time dependent relaxation is consistent with the following picture of partial PZT polarization. Initial application of 2 V begins to reorient the polarization of each PZT grain into the out of plane direction. With removal of the driving voltage, the polarization directions of the grains relax back to their original disordered lower energy state. This mechanism can be further verified through the implementation of simultaneous piezoresponse force microscopy and plasmonic near-field studies. With position dependent control of PZT polarization, as has been demonstrated using AFM,[42,43] such plasmonic memory gating could be employed for the creation of reconfigurable plasmonic nanocircuits without the need for continuous stimulus.

Our results demonstrate the effectiveness of PZT as a gate dielectric for control of graphene plasmons. The dramatic increase in tunability, arising from the large dielectric constant of PZT, minimizes the voltages necessary for significant modification of plasmonic response. Additionally, the potential for persistent modification of plasmonic properties with polarization of ferroelectric films presents the opportunity for creation of a variety of graphene based nanoplasmonic elements (circuits, reflectors, and lenses). Although losses are present in our device, exfoliation of graphene on atomically flat epitaxial PZT[44−46] could dramatically reduce unwanted plasmonic scattering, making PZT an ideal substrate for low voltage graphene based electronic applications.

■ ASSOCIATED CONTENT

Supporting Information

Electrical transport measurements on similar devices. Probe of hysteresis in graphene near-field signal. The Supporting Information is available free of charge on the ACS Publications website at DOI: 10.1021/acs.nanolett.5b00125.

■ AUTHOR INFORMATION

Corresponding Author

*E-mail: mgoldflam@ucsd.edu.

Notes

The authors declare no competing financial interest.

■ ACKNOWLEDGMENTS

This work is supported by ONR (N00014-13-1-0464). Instrument development at UCSD is supported by DOE-BES. B.Ö. acknowledges support by the NUS Young Investigator Award and the SMF-NUS Research Horizons Award 2009-Phase II. A.H.C.N. acknowledges the National Research Foundation, Prime Minister's Office, Singapore, under its Medium Sized Centre Programme and CRP award "Novel 2D materials with tailored properties: beyond graphene" (R-144-000-295-281).

■ REFERENCES

(1) Wagner, M.; Fei, Z.; McLeod, A. S.; Rodin, A. S.; Bao, W.; Iwinski, E. G.; Zhao, Z.; Goldflam, M.; Liu, M.; Dominguez, G.; et al. Ultrafast and Nanoscale Plasmonic Phenomena in Exfoliated Graphene Revealed by Infrared Pump-Probe Nanoscopy. *Nano Lett.* **2014**, *14*, 894−900.

(2) Li, Z. Q.; Henriksen, E. A.; Jiang, Z.; Hao, Z.; Martin, M. C.; Kim, P.; Stormer, H. L.; Basov, D. N. Dirac Charge Dynamics in Graphene by Infrared Spectroscopy. *Nat. Phys.* **2008**, *4*, 532−535.

(3) Frenzel, A. J.; Lui, C. H.; Fang, W.; Nair, N. L.; Herring, P. K.; Jarillo-Herrero, P.; Kong, J.; Gedik, N. Observation of Suppressed Terahertz Absorption in Photoexcited Graphene. *Appl. Phys. Lett.* **2013**, *102*, 113111.

(4) Grigorenko, A. N.; Polini, M.; Novoselov, K. S. Graphene Plasmonics. *Nat. Photonics* **2012**, *6*, 749−758.

(5) Fei, Z.; Rodin, A. S.; Andreev, G. O.; Bao, W.; McLeod, A. S.; Wagner, M.; Zhang, L. M.; Zhao, Z.; Thiemens, M.; Dominguez, G.; et al. Gate-Tuning of Graphene Plasmons Revealed by Infrared Nano-Imaging. *Nature* **2012**, *487*, 82−85.

(6) Geim, A. K.; Novoselov, K. S. The Rise of Graphene. *Nat. Mater.* **2007**, *6*, 183−191.

(7) Xue, J.; Sanchez-Yamagishi, J.; Bulmash, D.; Jacquod, P.; Deshpande, A.; Watanabe, K.; Taniguchi, T.; Jarillo-Herrero, P.; LeRoy, B. J. Scanning Tunnelling Microscopy and Spectroscopy of Ultra-Flat Graphene on Hexagonal Boron Nitride. *Nat. Mater.* **2011**, *10*, 282−285.

(8) Ahn, G.; Kim, H. R.; Ko, T. Y.; Choi, K.; Watanabe, K.; Taniguchi, T.; Hong, B. H.; Ryu, S. Optical Probing of the Electronic Interaction between Graphene and Hexagonal Boron Nitride. *ACS Nano* **2013**, *7*, 1533−1541.

(9) Zheng, Y.; Ni, G.-X.; Toh, C.-T.; Tan, C.-Y.; Yao, K.; Özyilmaz, B. Graphene Field-Effect Transistors with Ferroelectric Gating. *Phys. Rev. Lett.* **2010**, *105*, 166602.

(10) Zheng, Y.; Ni, G.-X.; Bae, S.; Cong, C.-X.; Kahya, O.; Toh, C.-T.; Kim, H. R.; Im, D.; Yu, T.; Ahn, J. H.; et al. Wafer-Scale Graphene/ferroelectric Hybrid Devices for Low-Voltage Electronics. *Europhys. Lett.* **2011**, *93*, 17002.

(11) Zheng, Y.; Ni, G.-X.; Toh, C.-T.; Zeng, M.-G.; Chen, S.-T.; Yao, K.; Özyilmaz, B. Gate-Controlled Nonvolatile Graphene-Ferroelectric Memory. *Appl. Phys. Lett.* **2009**, *94*, 163505.

(12) Hong, X.; Posadas, A.; Zou, K.; Ahn, C.; Zhu, J. High-Mobility Few-Layer Graphene Field Effect Transistors Fabricated on Epitaxial Ferroelectric Gate Oxides. *Phys. Rev. Lett.* **2009**, *102*, 2−5.

(13) Jandhyala, S.; Mordi, G.; Mao, D.; Ha, M.-W.; Quevedo-Lopez, M. A.; Gnade, B. E.; Kim, J. Graphene-Ferroelectric Hybrid Devices for Multi-Valued Memory System. *Appl. Phys. Lett.* **2013**, *103*, 022903.

(14) Jin, D.; Kumar, A.; Hung Fung, K.; Xu, J.; Fang, N. X. Terahertz Plasmonics in Ferroelectric-Gated Graphene. *Appl. Phys. Lett.* **2013**, *102*, 201118.

(15) Rajapitamahuni, A.; Hoffman, J.; Ahn, C.; Hong, X. Examining Graphene Field Effect Sensors for Ferroelectric Thin Film Studies. *Nano Lett.* **2013**, *13*, 4374−4379.

(16) Yusuf, M. H.; Nielsen, B.; Dawber, M.; Du, X. Extrinsic and Intrinsic Charge Trapping at the Graphene/ferroelectric Interface. *Nano Lett.* **2014**, *14*, 5437−5444.

(17) Baeumer, C.; Rogers, S.; Xu, R.; Martin, L.; Shim, M. Tunable Carrier Type and Density in Graphene/$PbZr_{0.2}Ti_{0.8}O_3$ Hybrid Structures through Ferroelectric Switching. *Nano Lett.* **2013**, *13*, 1693−1698.

(18) Hong, X.; Zou, K.; Dasilva, a. M.; Ahn, C. H.; Zhu, J. Integrating Functional Oxides with Graphene. *Solid State Commun.* **2012**, *152*, 1365−1374.

(19) Strikha, M. Modulation of Mid-IR Radiation by a Gated Graphene on Ferroelectric Substrate. *Ukr. J. Phys. Opt.* **2011**, *12*, 161.

(20) Keilmann, F.; Hillenbrand, R. Near-Field Microscopy by Elastic Light Scattering from a Tip. *Philos. Trans. Math. Phys. Eng. Sci.* **2004**, 787−805.

(21) Brehm, M.; Schliesser, A.; Cajko, F.; Tsukerman, I.; Keilmann, F. Antenna-Mediated Back-Scattering Efficiency in Infrared near-Field Microscopy. *Opt. Express* **2008**, *16*, 11203−11215.

(22) Bonnell, D. A.; Basov, D. N.; Bode, M.; Diebold, U.; Kalinin, S. V.; Madhavan, V.; Novotny, L.; Salmeron, M.; Schwarz, U. D.; Weiss, P. S. Imaging Physical Phenomena with Local Probes: From Electrons to Photons. *Rev. Mod. Phys.* **2012**, *84*, 1343−1381.

DOI: 10.1021/acs.nanolett.5b00125
Nano Lett. 2015, 15, 4859−4864

(23) Fei, Z.; Rodin, A. S.; Gannet, G.; Dai, S.; Regan, W.; Wagner, M.; Liu, M. K.; McLeod, A. S.; Dominguez, G.; Thiemens, M.; et al. Electronic and Plasmonic Phenomena at Graphene Grain Boundaries. *Nat. Nanotechnol.* **2013**, *8*, 821−825.
(24) Ocelic, N.; Huber, A.; Hillenbrand, R. Pseudoheterodyne Detection for Background-Free near-Field Spectroscopy. *Appl. Phys. Lett.* **2006**, *89*, 101124.
(25) Huber, A. J.; Ocelic, N.; Hillenbrand, R. Local Excitation and Interference of Surface Phonon Polaritons Studied by near-Field Infrared Microscopy. *J. Microsc.* **2008**, *229*, 389−395.
(26) Fei, Z.; Andreev, G. O.; Bao, W.; Zhang, L. M.; S McLeod, A.; Wang, C.; Stewart, M. K.; Zhao, Z.; Dominguez, G.; Thiemens, M.; et al. Infrared Nanoscopy of Dirac Plasmons at the Graphene-SiO_2 Interface. *Nano Lett.* **2011**, *11*, 4701−4705.
(27) Chen, J.; Badioli, M.; Alonso-González, P.; Thongrattanasiri, S.; Huth, F.; Osmond, J.; Spasenović, M.; Centeno, A.; Pesquera, A.; Godignon, P.; et al. Optical Nano-Imaging of Gate-Tunable Graphene Plasmons. *Nature* **2012**, *487*, 77−81.
(28) Caridad, J. M.; Rossella, F.; Bellani, V.; Maicas, M.; Patrini, M.; Díez, E. Effects of Particle Contamination and Substrate Interaction on the Raman Response of Unintentionally Doped Graphene. *J. Appl. Phys.* **2010**, *108*, 084321.
(29) Casiraghi, C.; Hartschuh, A.; Qian, H.; Piscanec, S.; Georgi, C.; Fasoli, A.; Novoselov, K. S.; Basko, D. M.; Ferrari, A. C. Raman Spectroscopy of Graphene Edges. *Nano Lett.* **2009**, *9*, 1433−1441.
(30) Dai, S.; Fei, Z.; Ma, Q.; Rodin, a S.; Wagner, M.; McLeod, a S.; Liu, M. K.; Gannett, W.; Regan, W.; Watanabe, K.; et al. Tunable Phonon Polaritons in Atomically Thin van Der Waals Crystals of Boron Nitride. *Science* **2014**, *343*, 1125−1129.
(31) Hwang, E. H.; Das Sarma, S. Dielectric Function, Screening, and Plasmons in Two-Dimensional Graphene. *Phys. Rev. B: Condens. Matter Mater. Phys.* **2007**, *75*, 1−6.
(32) Zhang, L. M.; Andreev, G. O.; Fei, Z.; McLeod, A. S.; Dominguez, G.; Thiemens, M.; Castro-Neto, A. H.; Basov, D. N.; Fogler, M. M. Near-Field Spectroscopy of Silicon Dioxide Thin Films. *Phys. Rev. B: Condens. Matter Mater. Phys.* **2012**, *85*, 075419.
(33) Hanson, G. W. Quasi-Transverse Electromagnetic Modes Supported by a Graphene Parallel-Plate Waveguide. *J. Appl. Phys.* **2008**, *104*, 084314.
(34) Woessner, A.; Lundeberg, M. B.; Gao, Y.; Principi, A.; Alonso-González, P.; Carrega, M.; Watanabe, K.; Taniguchi, T.; Vignale, G.; Polini, M.; et al. Highly Confined Low-Loss Plasmons in Graphene−boron Nitride Heterostructures. *Nat. Mater.* **2014**, *14*, 421−425.
(35) Basov, D. N.; Fogler, M. M.; Lanzara, A.; Wang, F.; Zhang, Y. Colloquium: Graphene Spectroscopy. *Rev. Mod. Phys.* **2014**, *86*, 959−994.
(36) Crassee, I.; Orlita, M.; Potemski, M.; Walter, A. L.; Ostler, M.; Seyller, T.; Gaponenko, I.; Chen, J.; Kuzmenko, A. B. Intrinsic Terahertz Plasmons and Magnetoplasmons in Large Scale Monolayer Graphene. *Nano Lett.* **2012**, *12*, 2470−2474.
(37) Kimmel, R.; Bruckstein, A. Regularized Laplacian Zero Crossings as Optimal Edge Integrators. *Int. J. Comput. Vis.* **2003**, *53*, 225−243.
(38) Frenzel, A.; Qazilbash, M.; Brehm, M.; Chae, B.-G.; Kim, B.-J.; Kim, H.-T.; Balatsky, A.; Keilmann, F.; Basov, D. Inhomogeneous Electronic State near the Insulator-to-Metal Transition in the Correlated Oxide VO_2. *Phys. Rev. B: Condens. Matter Mater. Phys.* **2009**, *80*, 1−7.
(39) Carminati, R.; Greffet, J.-J. Influence of Dielectric Contrast and Topography on the near Field Scattered by an Inhomogeneous Surface. *J. Opt. Soc. Am. A* **1995**, *12*, 2716.
(40) Hong, X.; Hoffman, J.; Posadas, A.; Zou, K.; Ahn, C. H.; Zhu, J. Unusual Resistance Hysteresis in N-Layer Graphene Field Effect Transistors Fabricated on Ferroelectric $Pb(Zr_{0.2}Ti_{0.8})O_3$. *Appl. Phys. Lett.* **2010**, *97*, 033114.
(41) Ni, G. X.; Zheng, Y.; Bae, S.; Tan, C. Y.; Kahya, O.; Wu, J.; Hong, B. H.; Yao, K.; Ö, B. Graphene-Ferroelectric Hybrid Structure for Flexible Transparent Electrodes. *ACS Nano* **2012**, *6*, 3935−3942.
(42) Gruverman, A.; Auciello, O.; Tokumoto, H. Scanning Force Microscopy for the Study of Domain Structure in Ferroelectric Thin Films. *J. Vac. Sci. Technol., B: Microelectron. Process. Phenom.* **1996**, *14*, 602−605.
(43) Paruch, P.; Tybell, T.; Triscone, J.-M. Nanoscale Control of Ferroelectric Polarization and Domain Size in Epitaxial $Pb(Zr_{0.2}Ti_{0.8})O_3$ Thin Films. *Appl. Phys. Lett.* **2001**, *79*, 530.
(44) Tybell, T.; Ahn, C. H.; Triscone, J.-M. Control and Imaging of Ferroelectric Domains over Large Areas with Nanometer Resolution in Atomically Smooth Epitaxial $Pb(Zr_{0.2}Ti_{0.8})O_3$ Thin Films. *Appl. Phys. Lett.* **1998**, *72*, 1454.
(45) Ahn, C. H.; Tybell, T.; Antognazza, L.; Char, K.; Hammond, R. H.; Beasley, M. R.; Fischer, O.; Triscone, J.-M. Local, Nonvolatile Electronic Writing of Epitaxial Pb $(Zr_{0.52}Ti_{0.48})O_3/SrRuO_3$ Heterostructures. *Science* **1997**, *276*, 1100−1103.
(46) Wang, Y.; Ganpule, C.; Liu, B. T.; Li, H.; Mori, K.; Hill, B.; Wuttig, M.; Ramesh, R.; Finder, J.; Yu, Z.; et al. Epitaxial Ferroelectric Pb(Zr, Ti)O_3 Thin Films on Si Using $SrTiO_3$ Template Layers. *Appl. Phys. Lett.* **2002**, *80*, 97.

DOI: 10.1021/acs.nanolett.5b00125
Nano Lett. 2015, 15, 4859−4864

Supporting information for "Tuning and persistent switching of graphene plasmons on a ferroelectric substrate"

Michael D. Goldflam[†*], *Guang-Xin Ni*[†,‡,$], *Kirk W. Post*[†], *Zhe Fei*[†], *Yuting Yeo*[$], *Jun You Tan*[$], *Aleksandr S. Rodin*[†‡], *Brian C. Chapler*[†], *Barbaros Özyilmaz*[‡,$], *Antonio H. Castro Neto*[‡], *Michael M. Fogler*[†], *D. N. Basov*[†]

† Physics Department, University of California, San Diego, La Jolla, CA 92093, USA
‡ Centre for Advanced 2D Materials and Graphene Research Centre, National University of Singapore, Singapore 117546
$ Department of Physics, National University of Singapore, 2 Science Drive 3, Singapore 117542

List of contents

1. Electrical transport measurement results

Electrical transport curves collected on four-terminal graphene field-effect transistor (GFET) devices on identical PZT substrates as those measured in near-field microscopy are shown in Fig S1. These R *vs.* V_G curves demonstrate the response of the GFET/PZT device in both the linear dielectric regime (Fig S1a: $-1V<V_G<1V$), as well as in the range where PZT begins to polarize (Fig S1b: $-2V<V_G<2V$). The data within the linear regime show one clearly defined maximum in resistance indicating a lack of polarization of the PZT film. In contrast, the larger sweep range reveals the existence of two maxima indicating partial polarization of the dielectric layer[1,2]. The observed anti-hysteresis in this transport data, as compared to the ferroelectric hysteresis we observed in our near-field data, is likely a result of different fabrication methods, taken to ensure compatibility with our near-field microscope and enable optimal plasmonic characterization. Specifically, the CVD graphene used for transport was wet transferred onto a PZT film. In contrast, for near-field measurements, graphene was exfoliated and dry transferred onto heated PZT to obtain optimally clean graphene, a necessity for clear plasmon propagation.

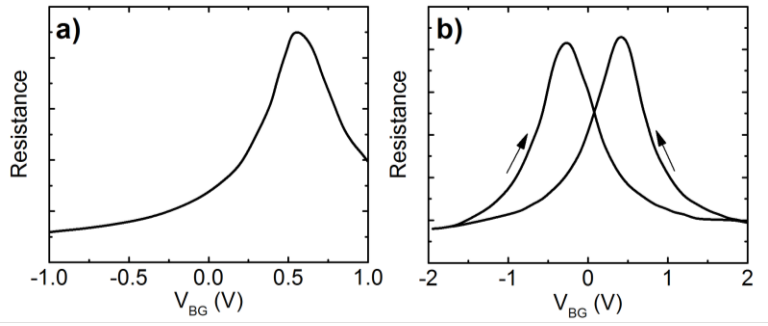

Figure S1: Dependence of graphene resistance on voltage sweep range in wet transferred CVD sample. a) Voltage sweep within the linear regime between -1V and 1V. b) Resistance measured during a voltage sweep from -2V to 2V.

2. Average near-field signal dependence on gate voltage

The hysteresis present in our near-field device can be observed by examining the voltage dependent normalized near-field signal of graphene, S(ω), which is given by the ratio of the graphene signal to that of PZT and is collected at a probing frequency of 890 cm^{-1}. In order to eliminate the effects of plasmonic reflection at the edge of graphene, these data are obtained in the interior regions of graphene, far from the edge. To account for topographic variation and changes in local properties of the samples, the values used in determining S(ω) are averages of the near-field signal obtained from images containing multiple PZT grains in each region of the device (graphene-covered and bare PZT). Identical areas were used at each voltage. As an analog to conventional transport data, we plot this data as 1/S(ω), which varies similarly with doping to graphene conductivity and is shown in Fig S2. These data, acquired for $0V<V_G<2V$, demonstrate the presence of a clear hysteresis between the two voltage sweep directions that is consistent with ferroelectric effects in our PZT film and also serve as a means of approximating the voltage of the charge neutrality point in our graphene sample. This V_{CNP} is obtained from the peak position in our 1/S(ω) data and yields a value in the range of 1V-1.5V.

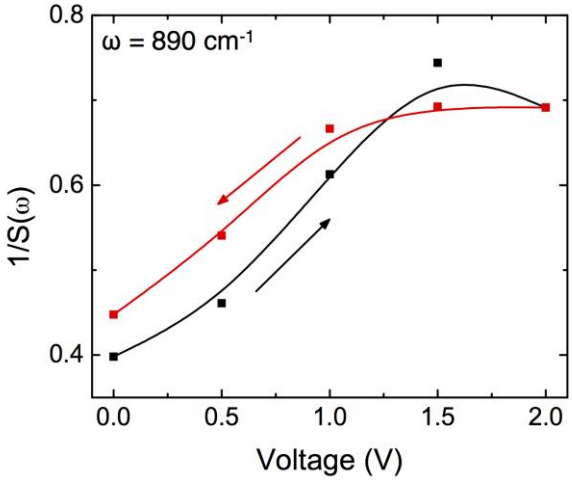

Figure S2: Voltage dependence of the normalized near-field signal in the interior of the graphene flake for backgate voltages between 0V and 2V

(1) Zheng, Y.; Ni, G.-X.; Bae, S.; Cong, C.-X.; Kahya, O.; Toh, C.-T.; Kim, H. R.; Im, D.; Yu, T.; Ahn, J. H.; *et al.* Wafer-Scale Graphene/ferroelectric Hybrid Devices for Low-Voltage Electronics. *Europhys. Lett.* **2011**, *93*, 17002.

(2) Hong, X.; Hoffman, J.; Posadas, A.; Zou, K.; Ahn, C. H.; Zhu, J. Unusual Resistance Hysteresis in N-Layer Graphene Field Effect Transistors Fabricated on Ferroelectric $Pb(Zr_{0.2}Ti_{0.8})O_3$. *Appl. Phys. Lett.* **2010**, *97*, 033114.